



# TU Tau B: The Peculiar “Eclipse” of a Possible Proto-barium Giant

Richard O. Gray<sup>1</sup>, Christopher J. Corbally<sup>2</sup>, Michael M. Briley<sup>1</sup>, Adam McKay<sup>1</sup>, Forrest Sims<sup>3</sup>, David Boyd<sup>4</sup>, Christophe Boussin<sup>5</sup>, Courtney E. McGahee<sup>1</sup>, Robert Buchheim<sup>6</sup>, Gary Walker<sup>7</sup>, David Iadevaia<sup>8</sup>, David Cejudo Fernandez<sup>9</sup>, Damien Lemay<sup>10</sup>, Jack Martin<sup>11</sup>, Jim Grubb<sup>12</sup>, Albert Stiewing<sup>13</sup>, Joseph Daglen<sup>14</sup>, Keith Shank<sup>15</sup>, Sydney Andrews<sup>1</sup>, Nick Barnhardt<sup>1</sup>, Rebekah Clark<sup>1</sup>, Hunter Corman<sup>1</sup>, Sabina Gomes<sup>1</sup>, Agastya Jonnalagadda<sup>1</sup>, Theo McDaries<sup>1</sup>, Ava Mills<sup>1</sup>, Will Newsom<sup>1</sup>, Andrew Slate<sup>1</sup>, and Michael Watts<sup>1</sup>

<sup>1</sup>Department of Physics and Astronomy, Appalachian State University Boone, NC 28608, USA

<sup>2</sup>Vatican Observatory Research Group, Steward Observatory, Tucson, AZ 85721-0065, USA

<sup>3</sup>Desert Celestial Observatory, Gilbert, AZ 85233, USA

<sup>4</sup>BAA Variable Star Section, West Challow Observatory, Wantage OX12 9TX, UK

<sup>5</sup>Observatoire de l’Eridan et de la Chevelure de Bérénice, F-02400 Épaux-Bézu, France

<sup>6</sup>Lost Gold Observatory, 8731 E. Lost Gold Cir, Gold Canyon, AZ 85118, USA

<sup>7</sup>Maria Mitchell Observatory, Minor Planet Center #811, 4 Vestal Street, Nantucket, MA 02554, USA

<sup>8</sup>Mountain View Observatory, 5700 N Avenida Observatory, Tucson, AZ 85750 USA

<sup>9</sup>Camino de las Canteras, 42, El Berruero E-28192, Spain

<sup>10</sup>10 Observatoire St-Anaclet, 195 Rang 4 Ouest, St-Anaclet, Quebec, G0K 1H0, Canada

<sup>11</sup>Huggins Spectroscopic Observatory, Rayleigh, Essex SS6 8AW, UK

<sup>12</sup>SAROS-1, 51000 Smith Road, Bradley, CA 93426 USA

<sup>13</sup>Desert Wing Observatory, 16210 N. Desert Holly Drive, Sun City, AZ 85351, USA

<sup>14</sup>Daglen Observatory, Mayhill, NM 88339, USA

<sup>15</sup>DEVO Observatory, Carrollton, TX 75007, USA

Received 2023 June 21; revised 2023 August 18; accepted 2023 August 18; published 2023 September 18

## Abstract

TU Tau (=HD 38218 = HIP 27135) is a binary system consisting of a C-N carbon star primary and an A-type secondary. We report on new photometry and spectroscopy which tracked the recent disappearance of the A-star secondary. The dimming of the A star was gradual and irregular, with one or more brief brightenings, implying the presence of nonhomogeneities in the carbon star outflow. We also present evidence that the A star is actively accreting *s*-process enriched material from the carbon star and suggest that it will therefore eventually evolve into a Barium giant. This is an important system as well because the A-type star can serve as a probe of the outer atmosphere of the carbon star.

*Unified Astronomy Thesaurus concepts:* [Eclipsing binary stars \(444\)](#); [Barium stars \(135\)](#); [A stars \(5\)](#); [Carbon stars \(199\)](#); [N stars \(1085\)](#); [S-process \(1419\)](#)

## 1. Introduction

TU Tau is a binary system consisting of a C-N type carbon star primary and an A-type secondary. The carbon star primary has extremely low flux in the blue violet, and so flux from the A-star companion can dominate in that part of the spectrum (see Figure 1). Sanford (1944) was the first to discover the composite nature of the spectrum of TU Tau. Barnbaum et al. (1996) classified the carbon star primary as C-N4<sup>+</sup> C<sub>2</sub>6, and the companion was classified by Richer (1972) as A2 III. We will update these classifications in Section 3.1. C-N giants show enhanced abundances of the *s*-process elements (such as strontium, yttrium, zirconium, and barium), and are believed to be asymptotic giant branch (AGB) stars. The carbon star in the TU Tau system is a semiregular variable (classified as SRb) with an approximate period of 190 days (Samus et al. 2017),<sup>16</sup> although Koen & Eyer (2002) report a period of 366 days.

Mason et al. (2001) attempted to resolve the binary using speckle interferometry, but failed, implying an angular

separation  $\rho \leq 0''.056$ . Kervella et al. (2019) included TU Tau in their study of binary stars using observed accelerations in the Gaia proper motions. Proper-motion accelerations are indeed observed in the Gaia data for TU Tau implying detection of the orbital motion, but the orbital characteristics, including the orbital period, are still undetermined. Nevertheless, Kervella et al. (2019) list estimates for the masses of the two components. For the primary, they derive a mass of  $4.05 \pm 0.2 M_{\odot}$ , which is reasonable for an AGB star, but the derived mass for the secondary is given as  $522^{+156}_{-78} M_{\text{jup}} \approx 0.5 M_{\odot}$ , which, as we will show in Section 3.2, is inconsistent with the spectral type of the secondary. Despite the fact that the orbital period is currently unknown, it is possible to compute a rough lower limit. van Belle et al. (2013) give an angular diameter for TU Tau A =  $3.894 \pm 0.011$  mas. Combining that with the Gaia DR3 parallax (Gaia Collaboration et al. 2022) =  $0.8482 \pm 0.0341$  mas yields  $R(\text{TU Tau A}) \approx 500 R_{\odot} \approx 2.3$  au. Assuming a total mass  $M_A + M_B = 7 M_{\odot}$  (see Section 3.2) and that the two stars are in contact, we derive  $P_{\text{min}} \approx 1.3$  yrs.

We will discuss evidence in Sections 3.1 and 4 that the A-star component is undergoing active accretion of material from the carbon star. As it turns out, the interaction goes the other direction as well. The A-star companion affects the infrared spectrum of the carbon star. Boersma et al. (2006) have detected unidentified infrared (UIR) emission due to fluorescence by polycyclic aromatic hydrocarbon (PAH) molecules in

<sup>16</sup> General Catalog of Variable Stars, June 2022 version <https://heasarc.gsfc.nasa.gov/W3Browse/all/gcvsv.html>.



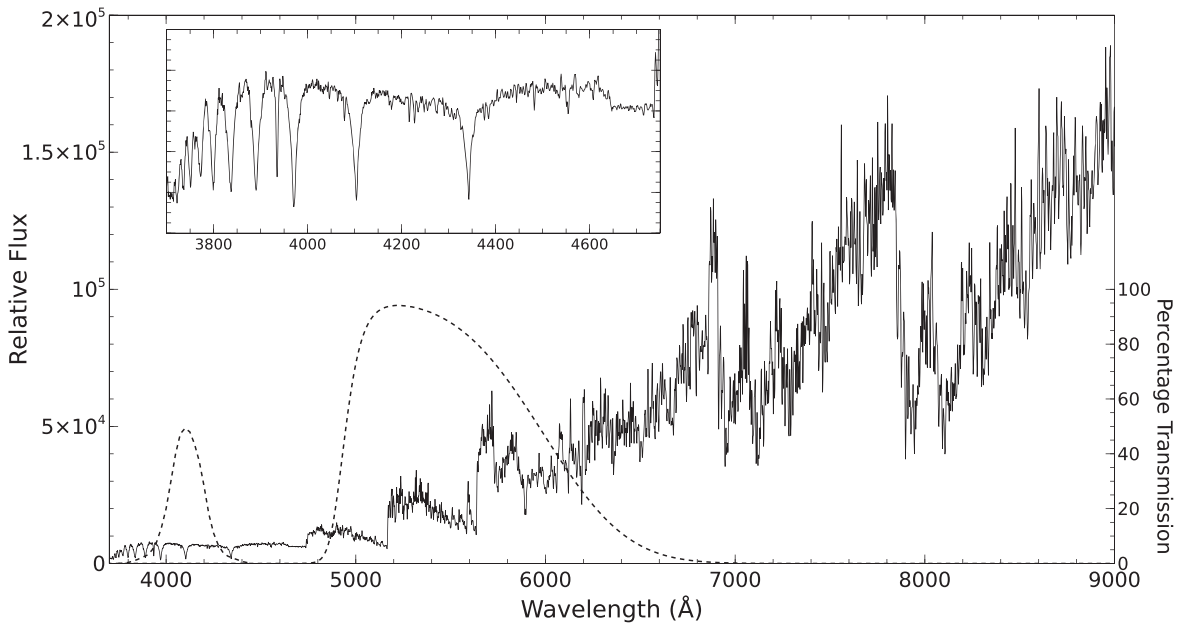


**Figure 1.** The LAMOST 2013 December 20, spectrum of TU Tau. Flux from the carbon star dominates at the longer wavelengths whereas the A-star companion (also shown in the inset) dominates in the blue violet. Also included in this plot are the passbands for the Strömgren- $v$  filter (dashed, centered near 4100 Å) and the Johnson- $V$  filter (dashed, centered near 5500 Å). It is clear that the flux through the Strömgren- $v$  filter is almost exclusively from the A-star companion. The flux through the Johnson- $V$  filter is dominated by the carbon star with a small contribution from the A-star companion.

the ISO SWS midinfrared spectrum of TU Tau. The UIR emission requires excitation by UV photons of the PAH molecules, and those photons are presumably provided by the A-star companion. The authors also argue that the UV photons from the companion may result in complex photochemistry in the ejecta from the carbon star. Reiter et al. (2015) published Spitzer/IRAC colors for TU Tau and note that it shows the largest IR excess for any of the semiregular variables in their sample.

Our study of TU Tau came about through an interest in discovering the progenitors of the barium giant stars. Barium giants are G- and K-type giants that show enhanced abundances of the  $s$ -process elements at an evolutionary stage well before the  $s$ -process elements are produced by neutron capture and dredged up to the surface. Usually,  $s$ -process enhancement occurs during the AGB evolutionary stage in C-N type carbon stars. For the barium stars, the prevailing theory for the origin of the  $s$ -process enhancements is external contamination via mass transfer to the current Ba star from an AGB companion that has now evolved to a white dwarf (McClure et al. 1980). Simple arguments based on evolutionary timescales and the orbital characteristics of Ba giants (North 2000) on the one hand, and white dwarf cooling times (Bohm-Vitense et al. 2000) on the other, suggest that most Ba giants must have been contaminated while on the main sequence. Since most Ba giants have masses  $\geq 2.0M_{\odot}$  (Escorza et al. 2017), this implies that on the main sequence these stars were B- or A-type. A search of carbon stars in the LAMOST (Wang et al. 1996) Data Release 7 spectrum database<sup>17</sup> revealed a number of C-N stars with A-type companions, including TU Tau. Remarkably, a close inspection of the spectrum of the A-star companion in the TU Tau system revealed an otherwise normal A-star with strong lines of Sr II, Ba II, and Y II, suggesting that it is a prime candidate for a barium giant progenitor (see Figure 2, top

spectrum). This prompted a campaign of spectroscopy and photometry, eventually involving not only the Dark Sky Observatory (Appalachian State University, North Carolina) and the Vatican Advanced Technology Telescope spectrograph, but also a number of amateur observatories which have made significant contributions to this research.

## 2. Observations

### 2.1. Photometry

Robotic CCD photometry of TU Tau in four bands, Strömgren- $v$  (S- $v$ , centered at 4100 Å), and Johnson-Cousins  $B$ ,  $V$ , and  $R_C$  has been carried out at Appalachian State University’s Dark Sky Observatory (DSO; situated in the Blue Ridge Mountains of North Carolina at an elevation of 1000 m) using the wide-field imager in the DSO-6 dome since 2021 October. That imager consists of a 300 mm  $f/4$  camera lens, and a filter wheel and CCD from Finger Lakes Instruments. The CCD chip is a KAF-16803. Full frame images cover a  $7^{\circ} \times 7^{\circ}$  field on the sky. The data are reduced with a pipeline using functions from the python `ccdproc` package (Craig et al. 2017). Differential aperture photometry is carried out with functions from the python library `photutils` (Bradley 2023). Exposures (S- $v$ :  $5 \times 90$  s, B:  $5 \times 90$  s, V:  $5 \times 45$  s, R:  $5 \times 10$  s) were obtained each clear night TU Tau could be observed. The comparison and check stars were TYC 1866-2430-1 (designated on the AAVSO chart as star “98”) and TYC 1866-990-1 (star “107”). The adopted magnitudes for those stars on the standard system (Henden 2009) are given in Table 1. The standard magnitudes for the S- $v$  band have not been determined for those comparison stars. However, the star HD 38334, which lies about  $15'$  from TU Tau has published Strömgren  $uvby$  photometry, which we use in Section 3.2 to estimate the intrinsic S- $v$  magnitude and by extension the absolute  $V$  magnitude of the A-star component.

<sup>17</sup> <http://www.lamost.org/lmusers/>

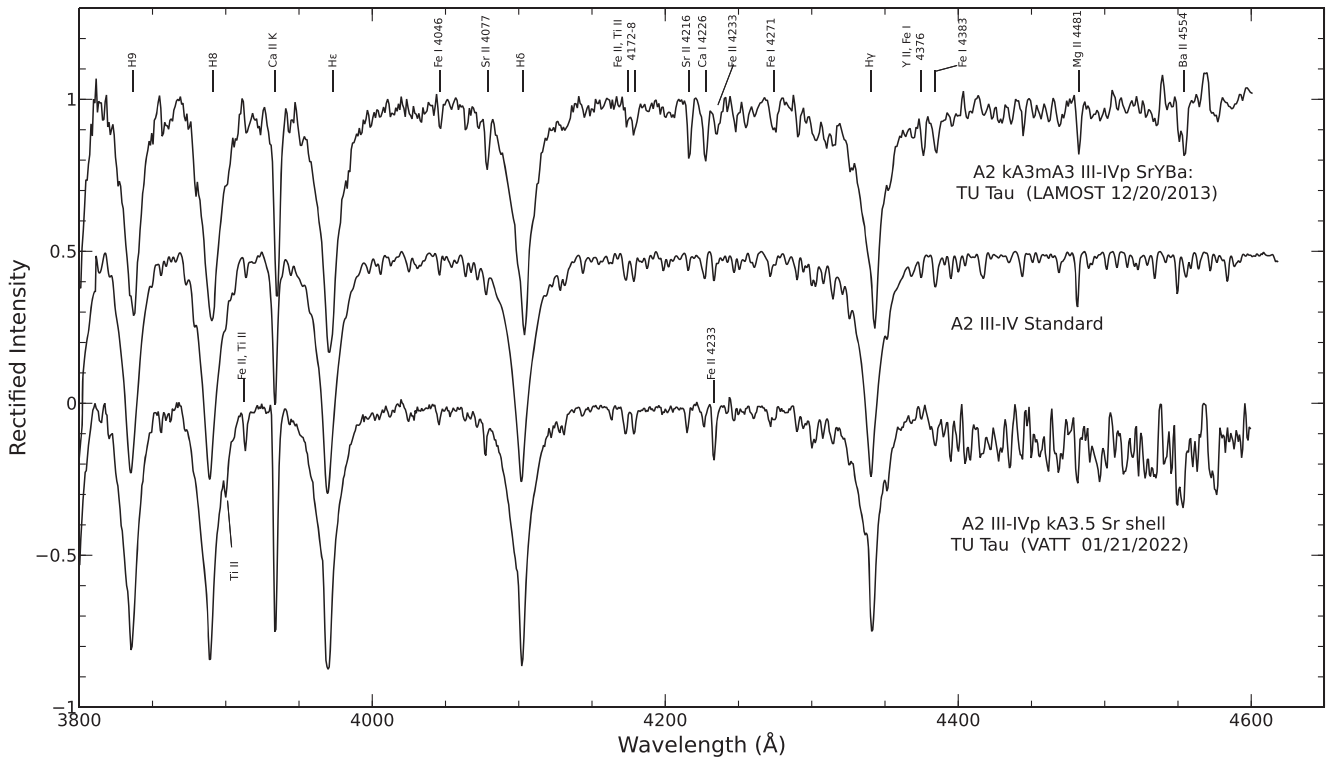


**Figure 2.** Top: the blue-violet portion of the LAMOST spectrum of TU Tau B showing the spectrum of the A-star companion in detail. Note the strong lines of *s*-process elements, including strontium, barium, and yttrium. Center: a standard A2 III-IV spectrum from the `libr18` standards library for comparison. Bottom: a spectrum of TU Tau B obtained with the Vatican Advanced Technology spectrograph on 2022 January 21. Note the strength of the Fe II  $\lambda 4233$  line. See Section 3.1 for more details on the classification of these spectra. All three spectra have been normalized to the continuum but the bottom two spectra have been displaced by 0.5 and 1.0 continuum units, respectively, for clarity.

**Table 1**  
Standard Johnson *B* and *V* Magnitudes

Filter	Star 98	Star 107
<i>B</i>	10.897 (0.060)	11.804 (0.069)
<i>V</i>	9.799 (0.004)	10.726 (0.054)

Table 2 lists the sources of *B*, *V*, and  $R_C$  photometry utilized for this study.

Figure 3 shows a plot of the differential Strömgren-*v* photometry obtained with the DSO-6 wide-field imager at the Dark Sky Observatory. The importance of Strömgren-*v* photometry is that the filter passband is centered on and confined to the region of the spectrum where the A-star companion dominates. The flux in the Johnson-*V* photometric band, on the other hand, is dominated by the carbon star (see Figure 1). It is clear that the Strömgren-*v* light curve shows a dramatic and irregular dimming of the A-type star commencing at about JD2459900. Figure 4 shows the Johnson-*V* light curve during the same time period.

## 2.2. Spectroscopy

Classification resolution spectroscopy ( $R \approx 1300$ ) of TU Tau has been obtained regularly using the GM spectrograph on the 0.8 m telescope at the Dark Sky Observatory since 2021 October. The  $600 \text{ g mm}^{-1}$  grating was utilized along with an Apogee camera with a blue-enhanced e2v chip with  $27 \mu\text{m}$  pixels (unbinned) to yield a spectral range from 3800 to 5700 Å. These spectra were reduced with a custom python pipeline which uses functions from `astropy` (The Astropy Collaboration et al. 2013, 2018, 2022) and

`ccdproc` (Craig et al. 2017). The pipeline employs optimal extraction of the spectra using the algorithm from Horne (1986) and detailed modeling of the sky background. Approximate flux calibration was carried out through the observation of several spectrophotometric standards most nights. The flux calibration was placed on an absolute scale using the Johnson *B* photometry from the DSO-6 wide-field imager.

In addition spectra were obtained on the 1.8 m Vatican Observatory Advanced Technology Telescope (Alice P. Lennon Telescope) employing the VATTspec, a  $1''$  slit, a  $600 \text{ g mm}^{-1}$  grating and a STA0520A back-thinned CCD with  $15 \mu\text{m}$  pixels, which yield a resolution of  $R = 3000$  and a spectral range of 3750–5500 Å. The VATTspec spectra were reduced with IRAF (Tody 1986, 1993) using standard procedures, and were approximately flux calibrated via the observation of a few spectrophotometric standards.

Spectra were also obtained at a number of amateur observatories listed in Table 3. These spectra were reduced using various packages designed for amateur use, including ISIS<sup>18</sup> and BASS.<sup>19</sup> Flux calibration was carried out using observations of standard stars and placed on an absolute scale via Johnson *V* photometry.

## 3. Discussion

### 3.1. Spectral Classification

During the period covered by this paper (2021 October–2023 April), the spectral type of the carbon-star component of TU Tau

<sup>18</sup> <http://www.astrosurf.com/buil/isis-software.html>

<sup>19</sup> <https://groups.io/g/BassSpectro>

**Table 2**  
Sources of  $B$ ,  $V$ , and  $R_C$  Photometry

Observatory	Telescope Diam (m)	Filters	Location	Observer	Abbreviation
Dark Sky Observatory	0.08	S-v, $B$ , $V$ , $R_C$	North Carolina	Richard Gray	DSO
AAVSONet BSM NH2	0.18	$B$ , $V$ , $R_C$	New Hampshire	Robert Buchheim	BHU
Sierra Remote Observatory	0.51	$V$	California	Gary Walker	WGR
Desert Celestial Observatory	0.1	$V$	Arizona	Forrest Sims	SFOA
Mountain View Observatory	0.1	$V$	Arizona	David Iadevaia	IDG
West Challow Observatory	0.36	$B$ , $V$ , $R_C$	UK	David Boyd	BDG
Observatorio El Gallinero	0.41	$B$ , $V$	Spain	David Cejudo Fernandez	CDZ
Observatoire St-Anaclet	0.36	$B$ , $V$ , $R_C$	Quebec	Damien Lemay	LMA

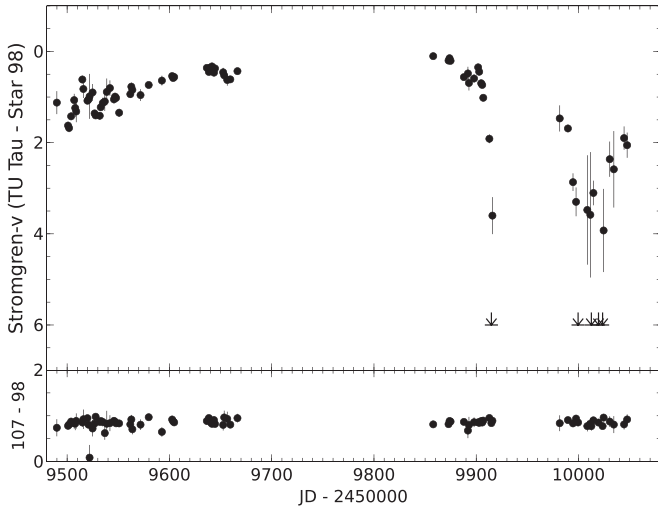


**Figure 3.** Strömgren  $v$ -band photometry (centered at  $4100 \text{ \AA}$ ) obtained with the wide-field imager at the Dark Sky Observatory. The top panel shows the photometry of TU Tau relative to the comparison star “98”, whereas the lower panel (on the same vertical scale) shows the magnitude difference between the comparison star (“98”) and the check star “107.” Five points in the upper panel are upper limits. TU Tau is not detected in those frames, even with a close visual inspection.

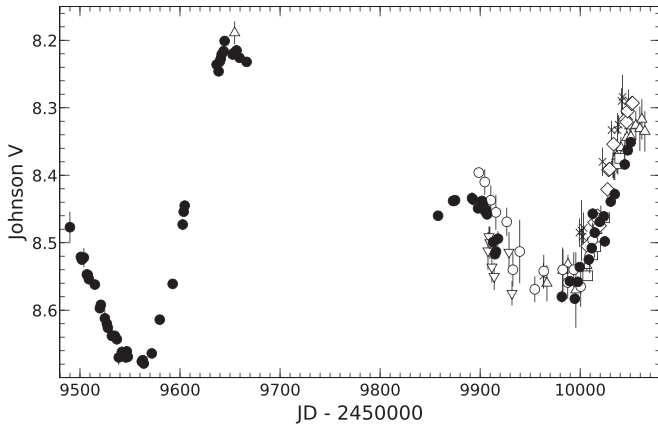


**Figure 4.** Johnson  $V$  photometry of TU Tau. The symbols refer to different observatories as follows:  $\bullet$ : DSO;  $\circ$ : BHU;  $\diamond$ : CDZ;  $\square$ : LMA;  $\triangle$ : SFOA;  $\nabla$ : WGR;  $\times$ : BDG. Some observers provided multiple closely spaced observations on a single night. These were averaged and the observational error was taken as the standard deviation of those data points.

(TU Tau A) remained unchanged even though the Johnson  $V$  magnitude varied by over half a magnitude. We agree with the spectral type reported by Barnbaum et al. (1996), C-N4<sup>+</sup> C<sub>2</sub>6.

On the other hand, the spectrum of the A-star component (TU Tau B) underwent some marked and interesting changes,

illustrated in Figure 2. In addition to the many spectra obtained at DSO ( $R = 1300$ ) and the observatories listed in Table 3, some of which have higher resolution than the DSO spectra, but very restricted spectral ranges, we have four higher resolution spectra which we can use to derive detailed spectral types for the A-type component. Three of these are from VATTspec ( $R = 3000$ ) and one from LAMOST ( $R = 1800$ ). The VATTspec spectra were obtained on 2021 October 25, 2022 January 21 and 2023 January 12. The LAMOST spectrum was acquired on 2013 December 20. We will begin with detailed comments on the VATTspec spectrum obtained on 2021 October 25, as it shows the least pronounced peculiarities.

Our spectral types are based on the standard classification criteria for A-type stars (Gray & Corbally 2009), which include the widths and strengths of the Balmer lines, the strength of the Ca II K line, and the strength of the general metallic-line spectrum.

These classifications were carried out in comparison with the standard stars in the MKCLASS library `libr18`<sup>20</sup>(Gray & Corbally 2014). All classifications reported here were carried out manually and did not utilize the automatic spectral classification program MKCLASS. However, we did employ the manual classification program `xclass`, which utilizes `libr18` and can interpolate between the standards in that library.

VATT 2021 October 10: the hydrogen-line wings as well as the general metallic-line spectrum are consistent with a spectral type of A2 III-IV for this spectrum of TU Tau B. However, there are a few ways in which this spectrum deviates from the standards. The Sr II  $\lambda 4077$  and  $\lambda 4216$  lines are both somewhat strong compared to the A2 III-IV standard. Likewise, the Fe II  $\lambda 4233$  line is stronger in this spectrum than in the A2 III-IV standard. A strong Fe II  $\lambda 4233$  line can indicate the presence of circumstellar gas and is a criterion for classifying a star as a “shell” star (see Gray & Corbally 2009, and the following paragraphs). In this case the Fe II  $\lambda 4233$  line is not strong enough to warrant a full “shell” classification. Another peculiarity is that the Ca II K line is stronger than for a normal A2 star; it is intermediate in strength between A2 and A3.

One of the most notable ways this spectrum deviates from the A2 III-IV standard, however, is in the hydrogen-line profiles. The wings of the hydrogen lines are in excellent agreement with the A2 III-IV standard, but all of the visible Balmer lines show narrow, slightly deep, and redshifted cores (see Figure 5). A difference spectrum (TU Tau B – A2 III-IV standard) for the H $\delta$  line shows that this redshifted core arises from an inverse P-Cygni profile (see Figure 5). An inverse

<sup>20</sup> <https://www.apstate.edu/~grayro/mkclass/>

**Table 3**  
Sources of TU Tau Spectroscopy

Observatory	Telescope Diam (m)	Spectrograph	Resolution	Spectral Range (Å)	Location	Observer	Abbreviation
Dark Sky Observatory	0.80	GM spectrograph	1300	3800–5700	North Carolina	various	DSO
Vatican Observatory	1.8	VATTspec	3000	3750–5500	Arizona	Christopher Corbally	VATT
LAMOST Observatory	4.0	Low Resolution mode	1800	3700–9000	Hebei, China	various	LAMOST
Lost Gold Observatory	0.41	Shelyak ALPY 600	500	3750–7250	Arizona	Robert Buchheim	LGO
Observatoire de l'Éridan et de la Chevelure de Bérénice	0.20	Shelyak ALPY 600	530	3700–7565	Épaux-Bézu, France	Christophe Boussin	OECB
West Challow Observatory	0.28	Shelyak LISA	1000	3900–7400	Wantage, UK	David Boyd	WCO
Desert Celestial Observatory	0.51	Shelyak LISA	1000	3750–7300	Arizona	Forrest Sims	DCO
Observatorio El Gallinero	0.31	Shelyak LISA	600	3900–7500	Madrid, Spain	David Cejudo Fernandez	OEG
SAROS-1	0.25	Shelyak UVEX	1400	3700–6900	California	Jim Grubb	SAROS
Huggins Spectroscopic Observatory	0.36	Shelyak LHIRES III	2000	3944–4939	UK	Jack Martin	HSO
Desert Wing Observatory	0.36	Shelyak LHIRES	14000	6482–6632	Arizona	Albert Stiewing	SALC
Daglen Observatory	0.36	Shelyak LHIRES III	14000	6333–6493	New Mexico	Joe Daglen	DO
DEVO Observatory	0.36	Shelyak LISA	1000	3850–7348	Texas	Keith Shank	DEVO

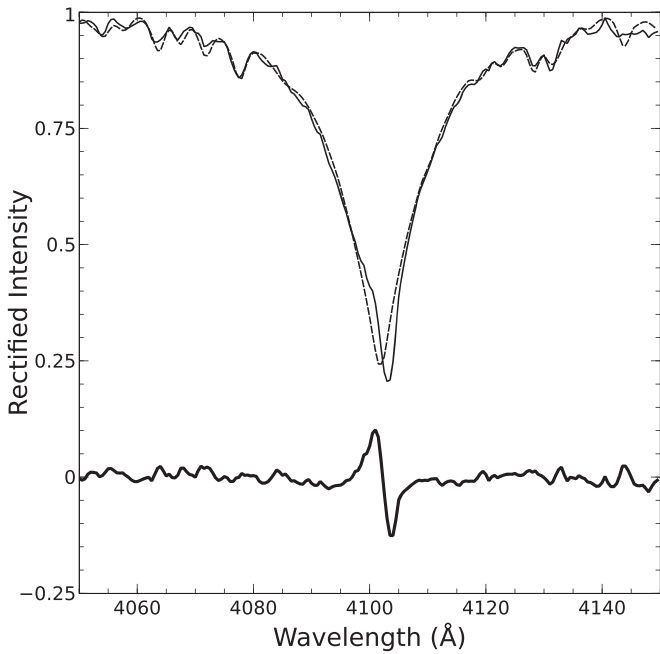


**Figure 5.** The solid line shows the  $H\delta$  profile of the 2021 October 10 VATT spectrum of TU Tau B. The dashed line shows the  $H\delta$  profile of the A2 III-IV standard. Both stars are represented in their rest frames. The redshifted core of TU Tau B is easily discerned. The bold solid line shows the difference spectrum (TU Tau B – A2 III-IV standard). What is revealed is an inverse P-Cygni profile, a spectroscopic signature of accretion. See Sections 3.1 and 4 for further details.

P-Cygni profile is an indication of active accretion of gas, and so is consistent with the shell nature of the star we deduced above. We will discuss the implications of this accretion in more detail in Section 4. The Ca II K line, in addition, shows a marked asymmetry and the core is also shifted to the red, probably also a consequence of accretion. We assign a spectral type A2 III-IVp kA2.5 (Sr) ((shell)) for this spectrum.

VATT 2022 January 21: the hydrogen-line wings and the general metallic-line spectrum are in good agreement with a spectral type of A2 III-IV. The metallic-line spectrum, however, shows more peculiarities than the 2021 October 10 spectrum. A few lines/blends appear weak (4143 Å and 4187 Å in particular, both dominated by Fe II). However, both Sr II  $\lambda 4077$  and  $\lambda 4216$  are stronger than normal. The Fe II  $\lambda 4233$  line is exceptionally strong. It is only in A supergiants and shell stars that Fe II  $\lambda 4233$  reaches this strength (see Gray & Corbally 2009). This suggests a “shell” classification for this spectrum. Such a classification is normally confirmed by examining the strength of the Fe II and Ti II lines in the “Fe II, Ti II forest” between  $H\gamma$  and 4500 Å, and the strengths of the Fe II multiplet 42 lines— $\lambda\lambda$  4924, 5018, 5169 (see Gray & Corbally 2009), but those spectral regions are obscured by the carbon star. However, two lines in the violet, Ti II  $\lambda 3900$  and Fe II, Ti II  $\lambda 3913$ , also enhanced in A-type shell stars, are unusually strong in this spectrum. This confirms our “shell” classification for this spectrum. The hydrogen-line profiles show the same asymmetries seen in the 2021 October 10 spectrum and a difference spectrum shows the same inverse P-Cygni profile (see Figure 6). The Ca II K line likewise is asymmetrical and redshifted. In this spectrum the total strength of the Ca II K line is intermediate to the A3 and A4 standards. This yields the spectral type A2 III-IVp kA3.5 Sr shell.

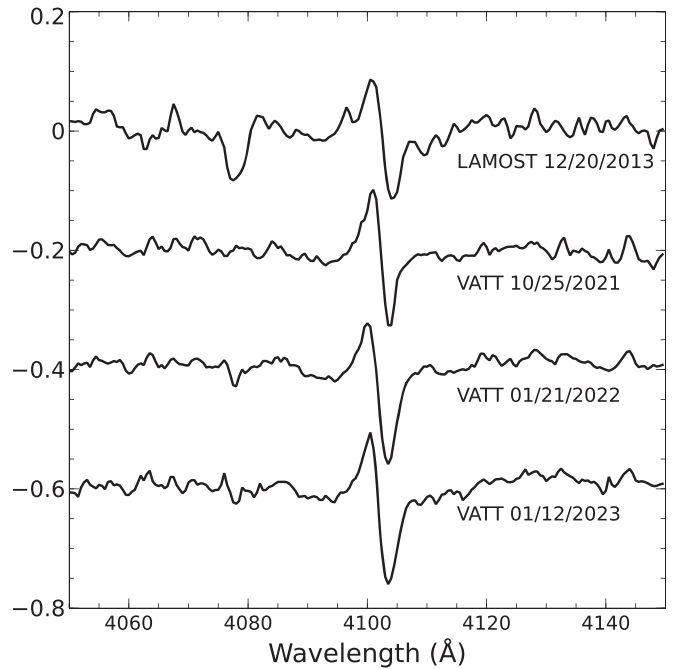


**Figure 6.** Difference spectra for the LAMOST spectrum and the three VATT spectra at  $H\delta$  (see Figure 5). Note that the inverse P Cygni profiles are all similar although some variation is visible. In the LAMOST difference spectrum, the feature at  $\lambda 4077$  arises from the much stronger Sr II  $\lambda 4077$  line in the LAMOST spectrum compared to the standard A2 III-IV spectrum.

**Table 4**  
Equivalent Widths (mÅ) of Selected Lines in TU Tau Spectra

Spectrum	Fe II, Ti II $\lambda 3913$	Sr II $\lambda 4077$	Sr II $\lambda 4216$	Ca I $\lambda 4226$	Fe II $\lambda 4233$
LAMOST (107807030)	blended	594	582	837	422:
VATT 10/25/21	206	215	217	245	302
VATT 01/21/22	302	233	211	213	444
VATT 01/12/23	264	197	249	225	343
A2 III-IV std	164	184	139	211	226

VATT 2023 January 12: this spectrum is similar to the 2022 January 21 spectrum, showing the same peculiarities and asymmetries. However, the shell lines noted above in the 2022 January 21 spectrum are somewhat weaker. This yields the spectral type A2 III-IVp kA3.5 Sr (shell).

LAMOST 2013 December 20: The LAMOST spectrum is the most peculiar of the four. The hydrogen-line wings agree with the A2 III-IV standard. However, the general metallic-line spectrum is stronger, and is more similar in strength to an A3 star than an A2. A number of lines are very strong. The Sr II  $\lambda 4077$  line is very strong, as is Sr II  $\lambda 4216$  (see Table 4). Lines of other *s*-process elements, Y II  $\lambda 4374$  and Ba II  $\lambda 4554$  (although that line may have a significant contribution from the carbon star) are also very strong. Interestingly, Ca I  $\lambda 4226$ , a resonance line of neutral calcium is also very strong. The Fe II  $\lambda 4233$  shell line has a broad profile but its core is not as deep as in the VATT 2022 January 21 spectrum, so the equivalent width recorded in Table 4 is uncertain. The hydrogen lines also show the same asymmetries displayed by the three VATT spectra, and a difference spectrum shows a clear inverse P-Cygni profile (Figure 6). The Ca II K line has a strength

similar to that of the A3 standard, but in this spectrum it has a symmetrical profile and is not redshifted. These considerations yield the spectral type: A2 kA3mA3 III-IVp SrYBa.

The most dramatic change in the spectrum of TU Tau, however, was the disappearance of the A star beginning in 2023 February. The dimming of this component was gradual and irregular and characterized by one or more brief reappearances. This phenomenon is discussed in Section 3.3.

### 3.2. Basic Physical Parameters

Our spectral types and Strömgren- $v$  photometry of the A-type companion allow a rough calculation of the basic physical parameters for the companion star, including the luminosity, mass, radius, and the effective temperature. Recall that the carbon star contributes negligible flux in the S- $v$  band. Our intermediate goal is to use the S- $v$  photometry for TU Tau B to derive an estimate for the absolute magnitude,  $M_V$ , of TU Tau B in the Johnson- $V$  band. This requires a number of steps. First, an examination of Figure 3 indicates that the brightness of the A-star companion varies. We will argue in Section 3.3 that the A-star companion is being obscured by clumps and shells of dust in the outflow from the carbon star. From that figure we can see that the A star is brightest on the night of JD2459857 and we assume that on that night the S- $v$  magnitude represents the minimally obscured brightness of the A star, modified only by the interstellar reddening in the direction of TU Tau plus a possible internal reddening along our line of sight to TU Tau B in the TU Tau system itself. To begin with we will ignore the internal reddening, but will attempt to estimate it later.

We begin by placing the S- $v$  photometry for TU Tau B on the night of JD2459857 on the standard system. This is done via the star HD 38334, an A3 star about 15' from TU Tau, which was observed on the same exposures of TU Tau taken with the wide-field DSO-6 imager. HD 38334 has been observed on the Strömgren system, with the following magnitudes:  $V = 7.96$ ,  $b-y = 0.118$ , and  $m_1 = 0.180$  (Perry & Johnston 1982). Using the definition of  $m_1 = (v - b) - (b - y)$  (where  $v$  corresponds to what we are calling S- $v$  in this paper) and the fact that Strömgren  $y$  is transformed to be on the same system as Johnson  $V$ , we determine that  $S-v(\text{HD 38334}) = 8.38 \pm 0.01$ . On the night of JD2459857, the differential magnitude in the S- $v$  band between TU Tau B and HD 38334 was  $3.340 \pm 0.028$  mag, yielding  $S-v(\text{TU Tau B}) = 11.72 \pm 0.03$ .

Note: in the calculations that follow, we have used a Monte Carlo method for the propagation of errors (Crowder et al. 2020), and have assumed that the errors of the observed quantities have Gaussian distributions.

The interstellar reddening at the distance and position of TU Tau can be estimated from the 3-D reddening map of Green et al. (2019):  $E(g - r) = 0.28_{-0.04}^{+0.03}$ . This can be converted to the color excess in the Johnson system using the formula in that reference:  $E(B-V) = 0.981E(g-r)$ . This yields  $E(B-V) = 0.27_{-0.04}^{+0.03}$ . The corresponding absorption in the S- $v$  band can be estimated by interpolating in the tabulation of  $A(\lambda)/A(V)$  in Table 21.6 of Cox (2000).  $A(V) = R_V E(B-V)$  where we take  $R_V$ , the ratio of total to selective absorption = 3.1, the typical value for the diffuse interstellar medium (cf. Cardelli et al. 1989).  $A(V)$  is the total absorption in magnitudes in the  $V$  band, whereas  $A(\lambda)$  is the corresponding total absorption in a band centered at wavelength  $\lambda$ . For the S- $v$  band,  $\lambda = 0.41 \mu\text{m} = 4100\text{\AA}$ . The reddening-free

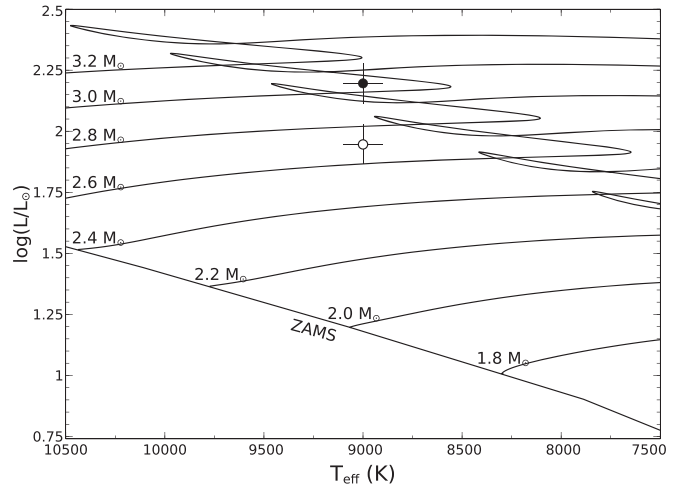


**Figure 7.** A theoretical HR diagram based on the  $Z = 0.02$  evolutionary tracks of Bressan et al. (2012) shows the position of the two solutions for TU Tau B discussed in Section 3.2. The point indicated by the open circle assumes no internal reddening in the TU Tau system. The filled circle indicates the solution for an internal reddening of  $E(B - V)_{\text{internal}} = 0.14$  (see text).

magnitude in the S- $v$  band,  $S-v_0$ , is given by  $S-v - A(0.41 \mu\text{m})$ . This yields  $S-v_0(\text{TU Tau B}) = 10.54 \pm 0.18$  as the reddening-free S- $v$  magnitude of TU Tau B (note again that at this point we are assuming that there is no internal reddening in the TU Tau system; this is unlikely, and we consider that question below). To use this to deduce the reddening-free Johnson- $V_0$  magnitude for TU Tau B, we must derive typical reddening-free Strömgren colors for an A2 III-IV star. This can be accomplished by pulling out lightly reddened stars from Gray & Garrison (1987) with similar spectral types to TU Tau B (A2 IV, A2 III-IV, A2 III). We find, for a typical A2 III-IV star,  $(b-y)_0 = 0.041 \pm 0.016$  and  $m_0 = 0.153 \pm 0.013$ . This gives  $V_0(\text{TU Tau B}) = 10.31 \pm 0.18$ . The Gaia DR3 parallax ( $0.8482 \pm 0.0341$  mas; Gaia Collaboration et al. 2016, 2022) for TU Tau yields  $M_V(\text{TU Tau B}) = -0.05 \pm 0.21$ .

The spectral-type, effective temperature calibration of Cox (2000) agrees with that of Gray & Corbally (2009) in assigning  $T_{\text{eff}} = 9000$  K for an A2 III-IV star. We estimate, from the precision of our spectral type, that the error in that determination is  $\pm 100$  K. The bolometric correction from Flower (1996) yields  $\log(L/L_\odot) = 1.946 \pm 0.080$  for the A-star companion. The solar-abundance ( $Z = 0.02$ ) evolutionary tracks of Bressan et al. (2012) imply  $M(\text{TU Tau B}) = 2.7 \pm 0.1 M_\odot$  (see Figure 7). This finally yields  $\log(g) = 3.70 \pm 0.08$  and  $R = 3.91 \pm 0.37 R_\odot$ .

Spectral synthesis based on ATLAS9 models (Castelli & Kurucz 2003) and the LTE spectral synthesis program SPECTRUM<sup>21</sup> (Gray & Corbally 1994), yields a best fit for the wings of the Balmer lines and lines of ionized species (Ti II, Fe II) at  $\log(g) = 3.5$ . This implies a slightly higher luminosity than calculated above which indicates that the internal reddening in the TU Tau system is not negligible. Setting  $E(B-V) = 0.27 + E(B-V)_{\text{internal}}$  and iterating to convergence gives  $E(B-V)_{\text{internal}} = 0.14$ ,  $\log(L/L_\odot) = 2.196 \pm 0.083$ ,  $\log(g) = 3.50 \pm 0.09$ ,  $M = 3.05 \pm 0.2 M_\odot$  and  $R = 5.18 \pm 0.51 R_\odot$ .

It is important to note that in principle this calculation could begin with the S- $v$  magnitude for TU Tau B on any night. The

<sup>21</sup> <https://www.appstate.edu/~grayro/spectrum/spectrum.html>

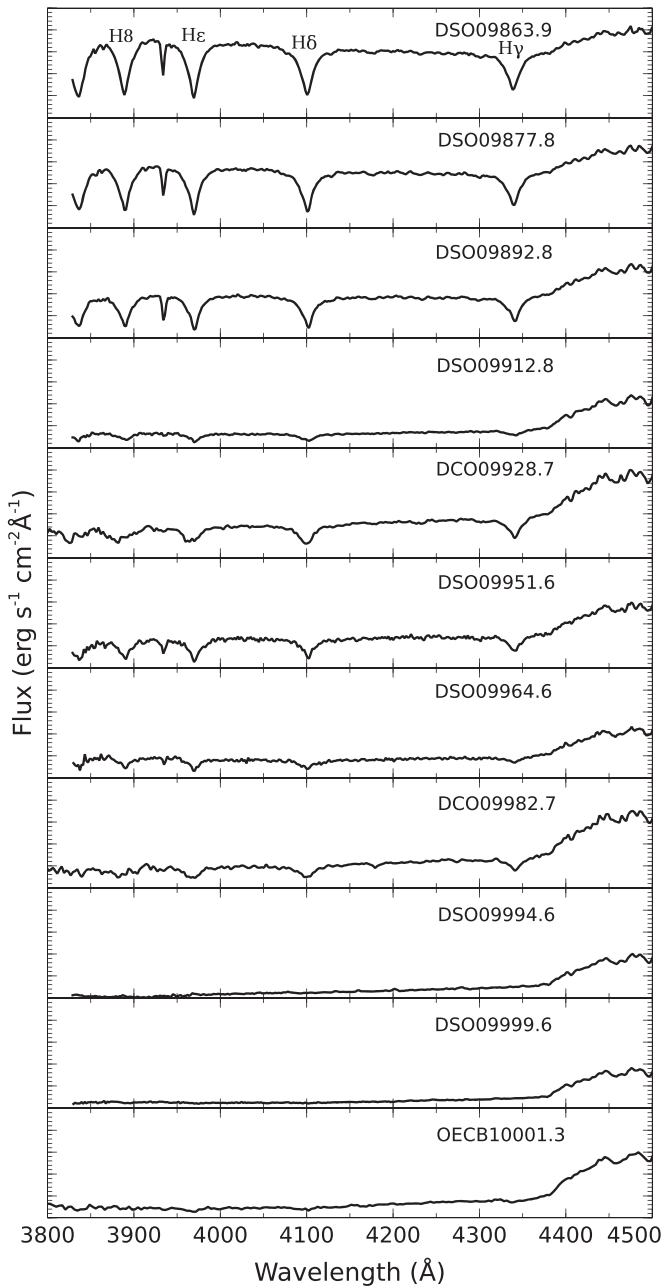


**Figure 8.** A montage of spectra of TU Tau in the blue-violet showing the region of the spectrum where the A-type companion is visible. In the first panel the Balmer lines (labeled) originating in that companion are clearly visible. The panel label indicates the origin of the spectrum (DSO: Dark Sky Observatory; DCO: Desert Celestial Observatory—Forrest Sims; OECEB: Observatoire de l’Eridan et de la Chevelure de Bérénice—Christophe Boussin) and the Julian date, in the format 2460000—JD. Each panel is scaled identically in flux, from 0 to  $2.5 \times 10^{-13}$  erg s $^{-1}$  cm $^{-2}$  Å $^{-1}$ . The montage begins with a spectrum taken on 2022 October 11 showing the A-type companion outside of the “eclipse”. Further spectra track the irregular dimming of the A-type companion through the last spectrum in the montage, obtained on 2023 February 25. Note the complete disappearance of the A-type companion between JD2459994 and 2459999. In the last spectrum close inspection reveals very weak absorption features at H $\delta$  and H $\epsilon$ . The montage continues in Figure 9.

choice of JD2459857 simply minimizes the internal reddening that we calculate for the line of sight to TU Tau B in the TU Tau system.

The first estimate of the temperature and luminosity of TU Tau B (assuming no internal reddening) places it in the upper main-sequence band (see Figure 7). The second estimate (with

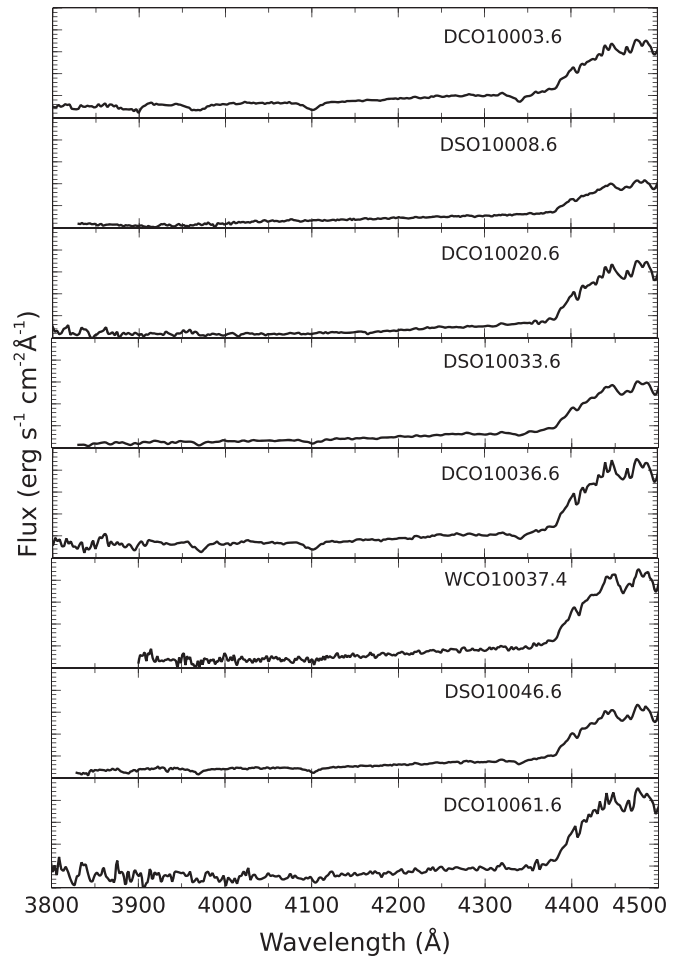


**Figure 9.** A continuation of the montage in Figure 8. The plots are scaled identically to that figure. The observatory codes are the same as that figure, except with the addition of WCO: West Challow Observatory—David Boyd. The A-type star remains faint in these spectra, although the visibility of that companion, as judged by the strength of the Balmer lines, is variable. Note the partial recovery in the visibility of the A-type companion in panel DCO10036.6. However, a fraction of a day later (panel WCO10037.4), the companion is not detected. By the end of the observing season (the end of 2023 April), the “eclipse” event is clearly still in progress (panel DCO10061.6).

$E(B - V)_{\text{internal}} = 0.14$ ) places the star near to the point of hydrogen exhaustion.

### 3.3. The “Eclipse” of TU Tau

The S-v light curve (Figure 3) and the montage of blue-violet spectra (Figures 8 and 9) document an unusual dimming, disappearance, and multiple partial reappearances of the A-star companion, which started about JD2459905. It is clear from those figures that this dimming event was not the result of a normal eclipse, as the A star disappeared and partially reappeared multiple times. By the end of the observational season, this event was still ongoing, with the A-type companion still quite faint.

The most plausible explanation for this unusual event is obscuration of the A-type companion by nonhomogeneities in the outer atmosphere of the carbon star, most probably related to dust formation in outflows. That the A-type companion is being obscured by dust is tentatively supported by the observation (see Figures 8 and 9) that the energy distribution of that star appears to get redder as it gets fainter. Two



scenarios seem equally plausible, as we know very little about the orbital dynamics of the binary system. The first scenario posits that the orbit of the A-type companion is inclined by an angle such that a grazing eclipse occurs during which the observer sees the A-type companion through the extended atmosphere of the carbon star. Dusty shells and other nonhomogeneities in the extended atmosphere are the cause of the “flickering” of the A-type companion that we have observed. Under this scenario, we should expect these dimming events to be periodic with the (currently unknown) orbital period of the A-type companion.

The alternative scenario is that the orbital period of the A-type star is sufficiently long so that we are not seeing the companion moving through or behind nonhomogeneities in the extended atmosphere of the carbon star. Rather, those nonhomogeneities are moving past the A-type star. Thus, under this scenario, the flickering of the A-type companion is caused by nonhomogeneities in the outflow from the carbon star passing in front of the A-type companion from the viewpoint of the observer. This suggests that these dimming events should occur at random intervals.

At the present time we cannot decide between these two scenarios, as there are only very sparse observational data for TU Tau B prior to this study. One data point we do have is provided by the spectrum of TU Tau published by Barnbaum et al. (1996) and acquired on 1995 February 15 (kindly provided in a private communication from Dr. Barnbaum). The A-type companion is not visible in that spectrum. Richer (1972) obtained a blue-violet spectrum of TU Tau that does show the A-type star at some point before the publication of that paper. Apart from that, we have been unable to find any other data that pertains to the visibility of the A-star companion in the literature. Archival spectra of TU Tau would be of value in deciding between these two scenarios. On the other hand, the S-*v* light curve of TU Tau (Figure 3) does show the A-type companion undergoing a slow brightening between JD2459489 and JD2459666. During that time the Johnson-*V* light curve (Figure 4) shows the carbon star going through a deep minimum. This suggests that during this period the A-type companion was “recovering” from a similar dimming event, perhaps occurring around JD2459300, hinting at a “period” of about 700 days. Further observations are required.

With our estimate for the *V* magnitude of TU Tau B derived in Section 3.2, it is possible to calculate the magnitude change for the entire system during a complete disappearance of the A-star component. This works out to be  $\Delta V \approx 0.1$ . This is consistent with the magnitude drop seen in Figure 4 at the beginning of the A-star disappearance (about JD2459900).

#### 4. Analysis and Conclusions

The results presented in this paper demonstrate that the A-type component of the TU Tau binary is interacting in a number of ways with the complex environment created by outflows from the carbon star. Not only is the ultraviolet flux from the A star inducing complex photochemistry in the carbon star outflow (see discussion in the Introduction), it is now clear from the inverse P-Cygni profiles seen in the difference spectra illustrated in Figures 5 and 6, that the A star is actively accreting gas from the outflow. That accretion has interesting implications for the evolution of the A star. C-N carbon stars, like the primary in the TU Tau system, have overabundances of carbon and *s*-process elements in their envelopes and

atmospheres, dredged up by deep convective currents from a layer that has undergone helium fusion. Those enhanced abundances will also be present in the outflows from the carbon star. It is clear, especially from the LAMOST spectrum of the A-type companion, which shows very strong lines of *s*-process elements, that the material accreting onto the surface of the A star is also enriched in those elements. This is exactly the scenario proposed by McClure et al. (1980) to explain the creation of Barium giants. Barium giants are G- and K-type giants that show large overabundances of *s*-process elements at a stage of evolution well before those elements are produced during shell helium burning. It is believed that those overabundances result from mass transfer of *s*-process enriched material from the carbon star to (what will become) the G/K-type companion. As far as can be determined, all Barium giants have white dwarf companions (Bohm-Vitense et al. 2000), thought to be remnants of the former carbon star. As Bohm-Vitense et al. (2000) argued (see Section 1), those Barium giants must have been contaminated while they were still on the main sequence (e.g., before hydrogen exhaustion). Since most Barium giants have masses  $M \geq 2.0M_{\odot}$  (Escorza et al. 2017), those stars were B- or A-type stars at the time of contamination. We have shown that the mass of the A-star component of TU Tau is  $\approx 3M_{\odot}$ . We have also shown clear evidence of active accretion of *s*-process enriched material onto the A-star companion. It thus appears that TU Tau B is a prime candidate for a Barium giant in-the-making.

There remain some questions about the nature of this accretion. Is the A star accreting material directly from the outflow from the carbon star, or has the carbon star filled its Roche lobe? This can be answered only when we learn more about the orbital dynamics of the system. We unfortunately are not able to observe the A star at H $\alpha$  or H $\beta$ , as the profiles of those lines might be diagnostic. However, observation of the A-star spectrum at higher resolution may help to elucidate the details of the accretion process. Analysis of the inverse P-Cygni profiles indicates that the velocity of the accretion inflow is on the order of  $200 \text{ km s}^{-1}$ . The shell lines, in particular Fe II 4233, are presumably formed via photoionization of the accreting material by ultraviolet photons from the A-type star itself. Analysis of the profile of that line in higher resolution spectra may reveal details of the velocity structure of the inflow and temporal changes in the accretion. Recall the rather broad, ill-defined profile of that line in the LAMOST spectrum (see Section 3.1) in contrast to the more narrow profiles in the VATT spectra.

Another open question arises from the relative strengths of the Sr II  $\lambda 4077$  and  $\lambda 4216$  lines. These are resonance lines of the strontium ion, and belong to the same multiplet. Because the *gf* (statistical weight  $\times$  oscillator strength) value of  $\lambda 4077$  exceeds that of  $\lambda 4216$  by a factor of two, the ratio of the equivalent widths of those lines,  $\text{EqW}(\text{Sr II } \lambda 4077)/\text{EqW}(\text{Sr II } \lambda 4216)$  should be  $>1$ . In the case of the A2 III-IV standard, that ratio  $\approx 1.32$  (see Table 4). However, that same ratio ranges from 0.79 to 1.10 in TU Tau. What that means is that if it is assumed those lines are formed exclusively in the photosphere of the star, those lines will give inconsistent strontium abundances. This will be the case even if strontium is distributed nonuniformly across the surface of the star. However, if the strontium lines are formed at least in part in the accreting material, then the peculiar ratios might be explained either through the velocity structure of that accreting

material or via a strontium abundance gradient in that material. This is because those two lines will be formed at different heights in that accreting flow, with the  $\lambda 4077$  line formed higher up than the  $\lambda 4216$  line. Only detailed modeling based on higher resolution and higher signal-to-noise spectra will be able to resolve this question.

We have suggested that the TU Tau system represents a stage in the evolutionary process that will result in a Barium giant star. Even if that is not the case, the TU Tau system is of great astrophysical interest, as the A-type companion acts as a probe of the outflows and outer atmosphere of the carbon star as shown graphically by the remarkable “flickering” of the A-type companion documented in Figure 3, and the montage in Figures 8 and 9. For that reason alone, TU Tau needs to be studied at higher resolution and over a longer period of time.

### Acknowledgments

We are grateful for the comments of an anonymous reviewer which have significantly improved this paper. This work has made use of data from the European Space Agency (ESA) mission Gaia (<https://www.cosmos.esa.int/gaia>), processed by the Gaia Data Processing and Analysis Consortium (DPAC; <https://www.cosmos.esa.int/web/gaia/dpac/consortium>).

Funding for the DPAC has been provided by national institutions, in particular the institutions participating in the Gaia Multilateral Agreement.

This work has used observations acquired at the Vatican Observatory Advanced Technology Telescope, Mt. Graham, Arizona.

This paper has made use of a spectrum from the Guoshoujing (LAMOST) telescope. The Guoshoujing Telescope (the Large Sky Area Multi-Object Fiber Spectroscopic Telescope; LAMOST) is a National Major Scientific Project built by the Chinese Academy of Sciences. Funding for the project has been provided by the National Development and Reform Commission. LAMOST is operated and managed by the National Astronomical Observatories, Chinese Academy of Sciences.

This work made use of Astropy (<http://www.astropy.org>): a community-developed core Python package and an ecosystem of tools and resources for astronomy (The Astropy Collaboration et al. 2013, 2018, 2022).

This research made use of ccdproc, an Astropy package for image reduction (Craig et al. 2017).




This research made use of Photutils, an Astropy package for detection and photometry of astronomical sources (Bradley 2023).

This research was made possible through the use of the AAVSO Photometric All-Sky Survey (APASS), funded by the Robert Martin Ayers Sciences Fund and NSF AST-1412587.

*Software:* Astropy (The Astropy Collaboration et al. 2013, 2018, 2022) ccdproc (Craig et al. 2017) SPECTRUM (Gray & Corbally 1994).

### ORCID iDs

Richard O. Gray  <https://orcid.org/0000-0001-7588-0477>  
 Christopher J. Corbally  <https://orcid.org/0000-0001-6797-887X>

Michael M. Briley  <https://orcid.org/0009-0005-0817-1183>  
 Adam McKay  <https://orcid.org/0000-0002-0622-2400>  
 Courtney E. McGahee  <https://orcid.org/0000-0001-6967-1142>

### References

- Barnbaum, C., Stone, R. P. S., & Keenan, P. C. 1996, *ApJS*, 105, 419  
 Boersma, C., Hony, S., & Tielens, A. G. G. M. 2006, *A&A*, 447, 213  
 Bohm-Vitense, E., Carpenter, K., Robinson, R., Ake, T., & Brown, J. 2000, *ApJ*, 533, 969  
 Bradley, L. 2023, *astropy/photutils*: v1.8.0, Zenodo, doi:10.5281/zenodo.7946442  
 Bressan, A., Marigo, P., Girardi, L., et al. 2012, *MNRAS*, 427, 127  
 Cardelli, J. A., Clayton, G. C., & Mathis, J. S. 1989, *ApJ*, 345, 245  
 Castelli, F., & Kurucz, R. L. 2003, in IAU Symp. 210, *Modelling of Stellar Atmospheres* (San Francisco, CA: ASP), A20  
 Cox, A. N. 2000, *Allen’s Astrophysical Quantities* (4th ed.; New York: Springer-Verlag)  
 Craig, M., Crawford, S., Seifert, M., et al. 2017, *astropy/ccdproc*: v1.3.0.post1, doi:10.5281/zenodo.1069648  
 Crowder, S., Delker, C., Forrest, E., & Martin, N. 2020, *Monte Carlo Methods for the Propagation of Uncertainties* (Cham: Springer Int. Publishing), 153  
 Escorza, A., Boffin, H. M. J., Jorissen, A., et al. 2017, *A&A*, 608, 100  
 Flower, P. J. 1996, *ApJ*, 469, 355  
 Gaia Collaboration, Prusti, T., & de Bruijne, J. H. J. 2016, *A&A*, 595, A1  
 Gaia Collaboration, Vallenari, A., Brown, A. G. A., et al. 2022, *Gaia Data Release 3: Summary of the Content and Survey Properties*, 2208, 00211, arXiv:2208.00211  
 Gray, R. O., & Corbally, C. J. 1994, *AJ*, 107, 742  
 Gray, R. O., & Corbally, C. J. 2009, *Stellar Spectral Classification* (Princeton, NJ: Princeton Univ. Press)  
 Gray, R. O., & Corbally, C. J. 2014, *AJ*, 147, 80  
 Gray, R. O., & Garrison, R. F. 1987, *ApJS*, 65, 581  
 Green, G. M., Schlafly, E., Zucker, C., Seagle, J. S., & Finkbeiner, D. 2019, *ApJ*, 887, 93  
 Henden, A. A., Welch, D. L., Terrell, D., & Levine, S. E. 2009, *AAS Meeting Abstracts*, 214, 407.02  
 Horne, K. 1986, *PASP*, 98, 609  
 Kervella, P., Arenou, F., Mignard, F., & Thevenin, F. 2019, *A&A*, 623, A72  
 Koen, C., & Eyer, L. 2002, *MNRAS*, 331, 45  
 Mason, B. D., Hartkopf, W. I., Holdenried, E. R., & Rafferty, T. J. 2001, *AJ*, 121, 3224  
 McClure, R. D., Fletcher, J. M., & Nemeč, J. M. 1980, *ApJ*, 238, L35  
 North, P. 2000, in *Int. Astronomical Union Symposia*, Vol. 177, *The Carbon Star Phenomenon*, Proceedings of the 177th Symposium of the International Astronomical Union, held in Antalya, Turkey, May 27-31, 1996, ed. R. F. Wing (Dordrecht: Kluwer Academic Publishers), 269  
 Perry, C. L., & Johnston, L. 1982, *ApJS*, 50, 451  
 Reiter, M., Marengo, M., Hora, J. L., & Fazio, G. G. 2015, *MNRAS*, 447, 3909  
 Richer, H. 1972, *ApJ*, 172, L63  
 Samus, N. N., Kazarovets, E. V., Durlevich, O. N., Kireeva, N. N., & Pastukhova, E. N. 2017, *ARep*, 61, 80  
 Sanford, R. F. 1944, *ApJ*, 99, 145  
 The Astropy Collaboration, Robitaille, Thomas P., Tollerud, Erik J., et al. 2013, *A&A*, 558, A33  
 The Astropy Collaboration, Price-Whelan, A. M., Lim, P. L., et al. 2022, *ApJ*, 935, 167  
 The Astropy Collaboration, Price-Whelan, A. M., Sipőcz, B. M., et al. 2018, *AJ*, 156, 123  
 Tody, D. 1986, *Proc. SPIE*, 627, 733  
 Tody, D. 1993, in *ASP Conf. Ser. 52, Astronomical Data Analysis Software and Systems II*, ed. R. J. Hanisch, R. J. V. Brissenden, & J. Barnes (San Francisco, CA: ASP), 173  
 van Belle, G. T., Paladini, C., Aringer, B., Hron, J., & Ciardi, D. 2013, *ApJ*, 775, 45  
 Wang, S.-G., Su, D.-Q., Chu, Y.-Q., Cui, X., & Wang, Y. 1996, *ApOpt*, 35, 5155